Dynamical switching of confined magnetic skyrmions under circular magnetic fields

S. Abdizadeh,[1,2] J. Abouie,[1] and Kh. Zakeri[2,*]

[1]*Department of Physics, Institute for Advanced Studies in Basic Sciences (IASBS), Zanjan 45137-66731, Iran*

[2]*Heisenberg Spin-dynamics Group, Physikalisches Institut, Karlsruhe Institute of Technology, Wolfgang-Gaede-Str. 1, D-76131 Karlsruhe, Germany*

(Received 12 August 2019; published 14 January 2020)

Understanding the dynamical properties of magnetic skyrmions is of prime importance for realization of skyrmion based devices. Here we report on the dynamics of a confined magnetic skyrmion under application of circular magnetic fields (CMFs). We provide the complex map of the dynamical states and demonstrate that under some conditions CMFs can change the skyrmion number and lead to the switching of the core polarity. Combing the results of micromagnetic simulations with those of analytical calculations, based on the extended Thiele equation, we unravel the physical mechanism behind this dynamical switching. The core switching is associated with the dynamical motions of the skyrmion driven by a CMF. The formation of domain walls and their movement from the border towards the center leads to shrinking of the skyrmion and the creation of a skyrmion with opposite core polarity. The results provide a guideline for checking the skyrmion's stability as well as an efficient way for switching the core polarity using CMFs.

DOI: 10.1103/PhysRevB.101.024409

I. INTRODUCTION

Skyrmions are nanoscale topological spin textures emerging in some chiral magnets. Owing to their fascinating physical and topological properties they have triggered a growing interest for application in modern information technology [1–8]. Recent observations of these topological objects at room temperature [7–11] and the need of rather small current densities [3,12–16] or magnetic field gradients [17,18] for their manipulation, compared to those needed for ordinary domain walls, has greatly enhanced the feasibility of using skyrmions for practical application, e.g., in race track memory devices.

Generally the presence of different competing magnetic interactions in a magnetic system can lead to a skyrmionic state [19–27]. Of particular interest are isolated skyrmions in confined geometries [28–38], since such structures can easily be fabricated using advance nanofabrication technologies [9–11]. The dynamics of such confined magnetic skyrmions has been extensively studied [38–42]. It has been shown that when the skyrmion is displaced from its equilibrium position, a restoring force causes the gyroscopic motion of the skyrmion around its equilibrium position [43,44]. Among the dynamic properties, the switching of the skyrmion core polarity has attracted special attention [45]. This is due to the fact that if the aim is to use the skyrmions as information carriers, e.g., in race track devices, it will be of prime importance to be able to define and switch their core polarity. The polarity can be switched by different means, e.g., polarized currents [46], magnetic [47], electric [48], or microwave [49] field pulses.

Here we present and unravel the complex dynamics of a confined magnetic skyrmion under a circular magnetic field (CMF) and illustrate an approach for switching of the core polarity. Switching a vortex core polarity using CMFs has already been demonstrated [50]. However, it is important to notice that a vortex is different from a skyrmion, and hence the switching process shall be entirely different. In the case of vortex core switching the dip formation near the core, which is interpreted as the excitation of nonlinear magnon modes, causes the switching of the vortex core polarity. However, the mechanism behind skyrmion core switching with CMFs is different. By performing extensive micromagnetic simulations we investigate the dynamics of a single magnetic skyrmion, constructed in a thin nanodisk. We demonstrate that the core polarity can be switched using CMFs and provide the H_0-ν_h dynamical map (H_0 and ν_h represent the amplitude and frequency of the field, respectively). We will show that the formation of domain walls and their movement from the border to the center cause the initial skyrmion to be quenched and immediately another skyrmion with opposite core polarity to be formed. We discuss the different regions of the dynamical map and demonstrate that under some circumstances, the switching of the core polarity can take place by a moderate magnetic field. The dynamical map contains also regions in which the skyrmion disappears and different orders, e.g., chiral domain walls separating magnetic domains, appear. We provide insights into this dynamical switching by combining the results of simulations with those of analytical calculations based on the generalized Thiele equation [44,51].

The paper is organized as follows. In Sec. II details of our micromagnetic simulations are provided. Section III is dedicated to the description of the analytical solution of the extended Thiele equation in the absence and presence of CMFs. In Sec. IV the results of the micromagnetic simulations are provided and are discussed by comparing them to those of the analytical calculations based on the generalized Thiele equation. Furthermore, additional discussion regarding the impact of the disk parameters on the dynamical map is presented. The possibility of switching a skyrmion with

*khalil.zakeri@partner.kit.edu

the skyrmion number of $Q = \pm 1$ to a skyrmionium with the skyrmion number of $Q = 0$ is discussed in detail. Finally, Sec. V provides a summary of the main results.

II. DETAILS OF MICROMAGNETIC SIMULATIONS

The numerical simulations were performed using the OOMMF code [52]. We considered a thin nanodisk with a thickness of $L = 0.6$ nm and a diameter of $2\mathcal{R} = 120$ nm. In order to form a single skyrmion in the disk, as the quasiground state, the Dzyaloshinskii-Moriya (DM) constant should be greater than $D_c = \frac{4}{\pi}\sqrt{KA}$, where K and A denote the magnetic anisotropy and exchange stiffness, respectively [30,53]. The values we used for our system are the ones used in Refs. [30,54–56]. The saturation magnetization was $M_s = 1.1 \times 10^6$ A/m, the exchange stiffness was $A = 16 \times 10^{-12}$ J/m, the DM constant was $D = 2.8 \times 10^{-3}$ J/m^2, the magnetic anisotropy constant was $K = 0.17 \times 10^6$ J/m^3, and the Gilbert damping constant was $\alpha_G = 0.03$. The disk was divided into cells of the size of $2.5 \times 2.5 \times 0.6$ nm^3. The quasiground state of a nanodisk with the above given parameters is a single skyrmion with up-core polarity located at the center of the nanodisk with the Bloch-type domain wall (Bloch skyrmion).

Prior to the application of any field, first the skyrmion was observed for 4 ns in order to ensure that an up-core skyrmion is fully stabilized in the center of the nanodisk.

A circular magnetic field (CMF) in the form of

$$\mathbf{H}(t) = H_0[\cos(\omega_h t)\hat{i} - \sin(\omega_h t)\hat{j}] \tag{1}$$

was then applied to the system, and its response was investigated over a wide range of H_0 and $\omega_h = 2\pi\nu_h$. Here H_0 and ν_h denote the amplitude and the frequency of the CMF, respectively.

As a general remark, atomistic simulations are more appropriate to describe the details of the switching phenomenon. However, the main idea here is to investigate the role of skyrmion motion (dynamics) upon application of the CMF on the switching. Such skyrmion dynamics can be well described using micromagnetic simulations. It will be shown that our results indicate that the skyrmion dynamics observed in the simulations can essentially be described by analytical trajectories calculated based on the Thiele equation. The micormagnetic simulations for the switching of the vortex core under application of magnetic fields has been discussed in Ref. [57]. It has been found that the calculated switching fields show a strong mesh dependence but nevertheless are of the order of magnitude of the experimental values at reasonable mesh sizes $a < \lambda$. Here λ denotes the exchange length. Hence we paid special attention to this issue. In our simulation the mesh size is $a = 2.5$ nm, which is smaller than the exchange length $\lambda = 4.5$ nm.

III. SOLUTION OF THE GENERALIZED THIELE EQUATION

A. Solution in the absence of a CMF

In the continuum limit, the dynamics of a single skyrmion is obtained by the generalized Thiele equation, in which the skyrmion is considered as a rigid particle [44,51]. For a massive skyrmion with the mass $\mathcal{M}$, in an environment with the gyrcoupling vector $\mathbf{G}$ and the dissipation tensor $\mathfrak{D}$, the Thiele equation reads as

$$\mathbf{G} \times \dot{\mathbf{R}} - \mathfrak{D}\dot{\mathbf{R}} - \mathcal{K}\mathbf{R} = \mathcal{M}\ddot{\mathbf{R}}, \tag{2}$$

where $\mathbf{R} = (x, y)$ is the position vector of the skyrmion guiding center and $\mathcal{K}$ is a restoring force constant arising from the environment in which the skyrmion is located. The gyrocoupling vector is given by $\mathbf{G} = (0, 0, \mathcal{G})$, where $\mathcal{G} = -4\pi Q M_s L/\gamma$. Here Q represents the skyrmion number and is given by

$$Q = \frac{1}{4\pi}\iint \mathbf{m} \cdot (\partial_x \mathbf{m} \times \partial_y \mathbf{m})\, dx\, dy, \tag{3}$$

where $\mathbf{m}$ denotes the local moments and Q represents both the winding number w and the core polarity p [1,56,58]. In analogous to $\mathcal{G}$ one can define the elements of the dissipative tensor $\mathfrak{D}_{ij}$. For $(i, j) = (x, x)$ and $(i, j) = (y, y)$ they can be simplified as $\mathfrak{D}_{ij} = \mathcal{D} = 4\pi\alpha_G \Gamma M_s L/\gamma$. Here Γ is given by

$$\Gamma = \Gamma_{ij} = \frac{1}{4\pi}\iint (\partial_i \mathbf{m} \cdot \partial_j \mathbf{m})\, dx\, dy, \quad (i, j) = (x, x), (y, y). \tag{4}$$

For $(i, j) = (x, y)$ and $(i, j) = (y, x)$ $\mathfrak{D}_{ij} = 0$. Considering a Cartesian coordinate Eq. (2) can be written in terms of x and y components. By defining a complex variable $S(t) = x(t) + iy(t)$ and substituting it into Eq. (2) one has

$$\mathcal{M}\ddot{S} + (\mathcal{D} - i\mathcal{G})\dot{S} + \mathcal{K}S = 0. \tag{5}$$

This is the equation of motion for a harmonic oscillator. In order to solve this equation we use the method of inspired guessing. We propose the following solution for $S(t)$:

$$S(t) = se^{-\varpi t}, \tag{6}$$

where s and ϖ are complex numbers and have to be determined. After substituting Eq. (6) into Eq. (5) and solving the second-order differential equation one finds the following solutions for ϖ:

$$\varpi_{1,2} = \frac{\mathcal{D} - i\mathcal{G}}{2\mathcal{M}} \pm \sqrt{\left(\frac{\mathcal{D} - i\mathcal{G}}{2\mathcal{M}}\right)^2 - \frac{\mathcal{K}}{\mathcal{M}}}. \tag{7}$$

Based on Eq (6), the imaginary part of ϖ shall provide the oscillatory movement and the real part shall give the dissipative part. We decompose $\varpi_{1,2}$ into the real and imaginary parts as $\varpi_{1,2} = \mathcal{D}_{1,2} + i\omega_{1,2}$. The final solution can then be written as

$$S(t) = s_1 e^{-i\omega_1 t} e^{-\mathcal{D}_1 t} + s_2 e^{-i\omega_2 t} e^{-\mathcal{D}_2 t}, \tag{8}$$

where s_1 and s_2 are complex numbers and are given by the initial conditions. ω_1, ω_2, $\mathcal{D}_1$, and $\mathcal{D}_2$ are real numbers and are given by

$$\omega_{1,2} = -\frac{\tilde{\mathcal{G}}}{2} \pm \sqrt{\mathcal{A}}, \quad \mathcal{D}_{1,2} = \frac{\tilde{\mathcal{D}}}{2} \mp \frac{\mathcal{B}}{2\sqrt{\mathcal{A}}}, \tag{9}$$

where

$$\tilde{\mathcal{D}} = \mathcal{D}/\mathcal{M},$$
$$\tilde{\mathcal{G}} = \mathcal{G}/\mathcal{M},$$
$$\mathcal{A} = \frac{\tilde{\mathcal{G}}^2}{4} + \tilde{\mathcal{K}} - \frac{\tilde{\mathcal{D}}^2}{4}, \quad \tilde{\mathcal{K}} = \mathcal{K}/\mathcal{M}, \tag{10}$$
$$\mathcal{B} = \frac{\tilde{\mathcal{G}}\tilde{\mathcal{D}}}{2}.$$

Later we will see that ω_1 and ω_2 are the eigenfrequencies of the skyrmion which, one may take either from the simulation or from the experiment. Equation (8) is the so-called general solution of the equation of motion, Eq. (5).

B. Solution in the presence of a CMF

The next step would be to apply a CMF and see how it influences the skyrmion dynamics. To this end, we add a clockwise CMF in the right-hand side of Eq. (5) and obtain the following equation:

$$\mathcal{M}\ddot{S} + (\mathcal{D} - i\mathcal{G})\dot{S} + \mathcal{K}S = \mu H_0 e^{-i\omega_h t}. \tag{11}$$

In the above equation μ is given by $\mu = \pi\mu_0\mathcal{R}LM_s\xi$, where μ_0 is the vacuum permeability and ξ is a constant being ≈ 1 [59–61]. We again use the method of inspired guessing. The proposed solution in this case would again be an oscillatory function in the form of

$$S(t) = s_1 e^{-i\omega_1 t} e^{-\mathcal{D}_1 t} + s_2 e^{-i\omega_2 t} e^{-\mathcal{D}_2 t} + f e^{-i\omega_h t}. \tag{12}$$

Here the first two terms represent the solution in the absence of the CMF, and the last term reflects the effect of the field. The factor f in its general form is a complex number and can be written as $f = |F|e^{i\varphi}$. Both $|F|$ and φ can be found by substituting the last term of Eq. (12) into Eq. (11). Doing so, one obtains the following equations for $|F|$ and φ:

$$|F| = \frac{\mu\tilde{H}_0}{\sqrt{\left(-\omega_h^2 - \omega_h\tilde{\mathcal{G}} + \tilde{\mathcal{K}}\right)^2 + \left(\tilde{\mathcal{D}}\omega_h\right)^2}},$$
$$\varphi = \arctan\left(\frac{\tilde{\mathcal{D}}\omega_h}{-\omega_h^2 - \omega_h\tilde{\mathcal{G}} + \tilde{\mathcal{K}}}\right). \tag{13}$$

Here $\tilde{H}_0$ is given by $\tilde{H}_0 = \frac{H_0}{M}$. The perfectors s_1 and s_2 are complex numbers. The initial conditions can uniquely specify the values of s_1 and s_2. We impose the following initial conditions on the problem:

$$S(t=0) = x_0 + iy_0 = 0, \quad \dot{S}(t=0) = 0. \tag{14}$$

At the end, the x and y coordinates of the skyrmion center during applying the field can be determined as the real and imaginary parts of S:

$$x(t) = \Re\{S(t)\}, \quad y(t) = \Im\{S(t)\}. \tag{15}$$

IV. RESULTS AND DISCUSSIONS

A. Results of micromagnetic simulations

We first stabilize a skyrmion in the nanodisk using the parameters discussed in Sec. II. The single Bloch skyrmion formed in this way has an up-core polarity and is located at the center of the nanodisk. In order to obtain the eigenmodes of the skyrmion, we apply a Gaussian pulse field with a width of 85 ps and a magnitude of about 104 kA/m to the system to shift the guiding center of the skyrmion over some distances ($x \approx 2$ nm, $y \approx 6$ nm). The guiding center gyrates about the center of the nanodisk in the counterclockwise direction. In order to avoid the effects caused by the field, the trajectory was recorded after 0.63 ns. In our simulation, we mesh the disk and find the guiding center of the skyrmion by focusing on the central region of the skyrmion with the local moments $m = m_z > 0$. The central point of this region is mathematically found during the time evolution.

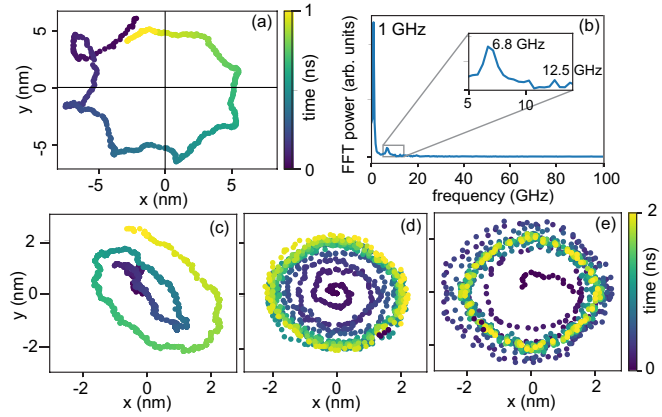

FIG. 1. (a) Trajectory of a confined skyrmion, recorded 0.63 ns after application of a Gaussian pulse field with a width of 85 ps and a magnitude of about 104 kA/m. (b) The FFT of the x and y components of the position of the skyrmion's guiding center. The skyrmion trajectory when a sine field with frequencies of (c) $\nu_1 = 1$, (d) $\nu_2 = 6.8$, and (e) $\nu_3 = 12.5$ GHz is applied to the system. The color bar shows the time evolution in the units of ns.

For a nanodisk with the material parameters of $M_s = 1.1 \times 10^6$ A/m, $A = 16 \times 10^{-12}$ J/m, $D = 2.8 \times 10^{-3}$ J/m^2, $K = 0.17 \times 10^6$ J/m^3, and $\alpha_G = 0.03$ the skyrmion trajectory and the eigenfrequencies are shown in Fig. 1. Since the skyrmion is massive, it possesses also a clockwise gyration mode so that the total trajectory is a polygon-like trajectory, as seen in Fig. 1(a). Performing a standard fast Fourier transformation (FFT) of the x and y coordinates of its guiding center, the eigenfrequencies of skyrmion were obtained to be $\nu_1 = 1$ GHz and $\nu_2 = 6.8$ GHz, and one small peak at about $\nu_3 = 12.5$ GHz [see Fig. 1(b)]. In order to distinguish between the clockwise and counterclockwise modes, sinusoidal fields with the frequencies equal to those observed as peaks in the FFT results were applied along the x direction. It turned out that the skyrmion undergoes a counterclockwise circular motion at $\nu_1 = 1$ GHz ([Fig. 1(c)]), a clockwise motion at $\nu_2 = 6.8$ GHz [Fig. 1(d)], and again a clockwise motion at $\nu_3 = 12.5$ GHz [Fig. 1(e)] around the center. While the first two frequencies are the well-known eigenmodes of the system, the third one which can mainly be excited with high-frequency fields is very likely the result of a more complex dynamics [1,58].

Now, our idea is to couple a CMF with a clockwise helicity to this up-core skyrmion and drive its dynamics. Since the clockwise motion is the natural low-frequency dynamics of a down-core skyrmion, one may be able to switch the skyrmion

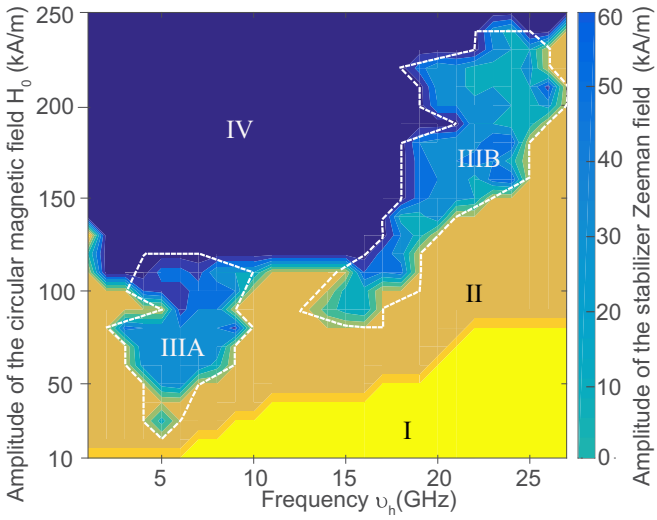

FIG. 2. The map of dynamical states of a skyrmion subjected to a clockwise CMF. The vertical axis represents the amplitude, and the horizontal axis represents the frequency of the CMF. In region I the skyrmion rotates in the clockwise direction without changes in its skyrmion number Q. It does not collide with the border within 20 ns. In region II the skyrmion rotates in the clockwise direction without changes in its Q, but it collides with the border within this time. In regions III and IV the sign of Q changes while applying the CMF. Region III is the switching region in which a skyrmion with an opposite core polarity can be achieved. In some cases a Zeeman field along the core direction of the initial skyrmion is needed to stabilize this skyrmion. The magnitude of this field is given as the color bar. Note that the color bar applies only to the region III. In region IV the skyrmion collides with the border, and chiral spin textures are created. The yellow, dark yellow, and dark blue represent regions I, II, and IV, respectively. In these regions no stabilizer field was applied at all.

in this way. The most intuitive explanation for the choice of a CMF is as follows. A CMF with the right helicity can in principle transfer the required angular momentum to a helical system to invert all the spins and consequently switch its Q number. Looking from the perspective of a rigid particle picture, the most straightforward way to excite the eigenmotion of a skyrmion would be a CMF with the right helicity, as such a field can couple to the skyrmion motion. The mathematical explanation comes from the solution of the Thiele equation in the presence of the field (see Sec. III B). This equation has analytical solutions in the form of harmonic oscillators in the presence of CMFs.

The skyrmion was subjected to a CMF in the form of Eq. (1), and its dynamics was investigated. First, the system was observed for 4 ns in order to ensure that an up-core skyrmion is fully stabilized in the center of the nanodisk. The CMF was then applied to the skyrmion, and the response of the system was investigated in great details and over a wide range of H_0 and ν_h. The resulting H_0-ν_h dynamical map is presented in Fig. 2, indicating a rather complex behavior of the skyrmion. Of particular interest is the time evolution of the skyrmion number during a CMF. Note that Q represents both the winding number w and the core polarity p [1,56,58].

Generally one identifies four main regions in the dynamical map, as indicated in Fig. 2. The most simplest one is the region I, where the skyrmion just follows the CMF. In region II the skyrmion starts to move with the field but it collides with the border of the disk and transforms into magnetic domains, separated with a Bloch wall. Careful analysis of Q of these textures indicate that they possess nearly the same Q as the one of the initial skyrmion. In region III the up-core skyrmion changes its skyrmion number and can eventually be switched to a down-core skyrmion before it collides with the border. Finally in region IV the skyrmion at the very first moment collides with the border, and other types of magnetic states are created which exhibit an opposite sign of Q (see the discussion below).

In region I as soon as the CMF is applied the skyrmion rotates with the field in a clockwise direction without any noticeable distortion. During the motion there is no collision with the border, and after 20 ns one still observes the initial skyrmion. Calculating the skyrmion number during the CMF indicates that it is $+0.89$. We call this region as the stability region in which the skyrmion remains stable during the field. This region is shown in yellow in Fig. 2. From the application point of view such a region is useful when the idea is to use the dynamics of skyrmions without having them affected by the CMF.

While in region I the skyrmion remains for 20 ns within the disk, in the region II the skyrmion rotates around the center for less than 20 ns, and it collides with the border. However, the sign of Q remains unchanged. This region is shown in dark yellow in Fig. 2. The difference between regions I and II is the time during which the skyrmion stays within the disk.

In region III, shown in light-blue/green in Fig. 2, the sign of Q is changed during the application of the CMF, and hence a skyrmion with an opposite sign of Q can be achieved. The simulations indicate that the value of Q changes from 0.89 to about -0.8. We call this region the switching region. As is apparent from Fig. 2 the switching between two distinct skyrmion numbers occurs over a large range of ν_h and H_0. However, one realizes that this region may be classified into two subregions. Subregion IIIA is located in the mid-frequency regime, near the eigenfrequency of the skyrmion, which describes its clockwise motion (in the absence of the field). Subregion IIIB is located at higher frequencies. In Fig. 3 two examples, representing these two subregions, are presented. Snapshots of the skyrmion are shown while the CMF is applied. Although the switching takes place in both subregions, the switching mechanism seems to be slightly different. Figure 3(a) presents the case of $H_0 = 30$ kA/m and $\nu_h = 5$ GHz. At $t = 4$ ns the CMF is applied the skyrmion starts to rotate in the field direction, and its radius becomes smaller. After 0.54 ns the initial skyrmion disappears, and a skyrmion with an opposite polarity appears in the disk. A similar process takes place in subregion IIIB. The example at $H_0 = 190$ kA/m and $\nu_h = 25$ GHz is shown in Fig. 3(b).

In order to unravel the underlying physical mechanism responsible for the switching and the timescales involved in the switching process one may investigate the change in Q during the CMF. The evolution of Q during the first 3 ns after application of the CMF for two points in the dynamical map representing the two subregions is presented in Fig. 3(c). For

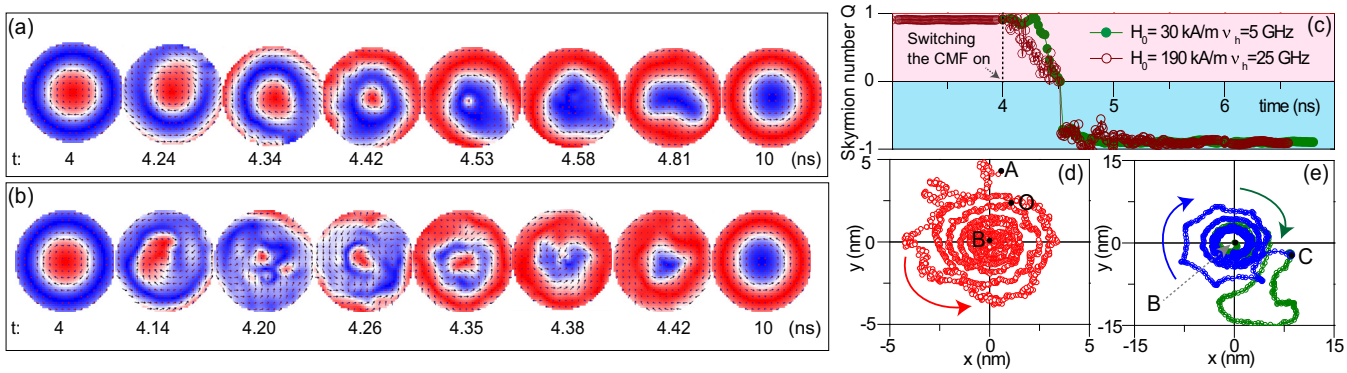

FIG. 3. The skyrmion is initially stabilized in the disk for 4 ns. It is then subjected to a clockwise CMF with (a) $H_0 = 30$ kA/m and $\nu_h = 5$ GHz and (b) $H_0 = 190$ kA/m and $\nu_h = 25$ GHz. The CMF is turned off at $t = 4.54$ ns in (a) and at $t = 4.4$ ns in (b). After turning the CMF off this skyrmion gyrates in a clockwise direction and is finally stopped at the center. The color scale indicates the direction of the local magnetic moments along the z direction, perpendicular to the disk (red: up, blue: down). Arrows represent the transverse components of local moments. (c) The time evolution of the skyrmion number during the CMF. (d) The trajectory of the skyrmion before the CMF is applied. The initial position of the skyrmion is first defined to be at point O ($x_0 = 1$ nm, $y_0 = 2$ nm). In order to avoid effects caused by deformations and breathing, the data are recorded from point A where the skyrmion's shape is rather circular. The skyrmion rotates counterclockwise and finally stops near the disk center (point B). (e) The trajectory of the skyrmion during and after application of the CMF ($H_0 = 30$ kA/m, $\nu_h = 5$ GHz). During the field the skyrmion rotates in clockwise direction from point B to C. At point C the up-core skyrmion switches to a down-core one. At this point the CMF is turned off. The down-core skyrmion rotates in a clockwise direction and finally stops at the center. Arrows indicate the direction.

$\nu_h = 5$ GHz and $H_0 = 30$ kA/m (subregion IIIA) the change in the sign of Q happens 0.54 ns after the CMF is applied, meaning that at this time the skyrmion is switched. Hence an efficient way to switch the skyrmion would be to switch off the CMF at this time and let the skyrmion be stabilized. For $\nu_h = 25$ GHz and $H_0 = 190$ kA/m (subregion IIIB) the first change in the sign of Q happens at 0.4 ns [see Fig. 3(b)]. This means that switching the CMF off at 0.4 ns would result in a skyrmion with opposite core polarity.

The time evolution of the skyrmion number should, in principle, exhibit an abrupt change during the switching. In fact, this has been partially observed in several points or regions of the dynamical map of the system [see, for example, Figs. 3(c)]. The apparent continuous change of Q is due to the following reasons. (1) The micromagnetic simulations can describe the systems with slowly varying magnetization distribution very well. However, they cannot describe precisely the details of the switching phenomenon, which is essentially an instant process in the view point of the slow dynamics. (2) The evolution of the Q number reported here is the results of "averaging" over the whole disk. The rapid change in spin configuration and appearance of domains near the edges leads to an apparent smooth change of Q in the vicinity of the switching. The skyrmion number is calculated based on the integral given in Eq. (3). The continuous change of Q with time is a result of the numerical integration over the whole disk area. What is important and can be safely concluded from such data analysis is the presence or absence of a sign change in Q with time upon application of the CMF.

The difference between subregions IIIA and IIIB is as follows. In the former case the shape of the skyrmion remains almost unchanged during the switching. It follows the field direction with a well-defined trajectory before it switches. In the latter case after application of the CMF the skyrmion starts to rotate around the disk center with a rather high speed, and during the rotation its size and shape change before it switches. One would therefore expect that in subregion IIIA the switching is entirely mediated by the coupling of the CMF to the clockwise motion of the skyrmion. In subregion IIIB, however, excitations of other types of modes related to the skyrmion deformation and breathing are also involved in the switching.

Note that in region III it is of prime importance to carefully analyze the time evolution of Q during the CMF as well as the position of the skyrmion within the disk. In the case that this skyrmion is nearly centered, it can stay for a relatively long time in the disk and would follow the CMF. However, if this skyrmion is far off-center or has an irregular shape, one would require a Zeeman field along the core direction of the initial skyrmion to stabilize the switched skyrmion at the center. The value of the stabilizer field is given in Fig. 2 as the color bar.

Now let us briefly discuss the role of the stabilizer field in region III. The position of the skyrmion is governed by the dynamics. As soon as the initial skyrmion is subjected to the CMF, it starts to move. The movement is governed by the amplitude and the frequency of the CMF. At a certain time (and position) the skyrmion polarity is switched and another skyrmion is created. If this switching takes place near the center of the nanodisk, the skyrmion will move around the center of the nanodisk and finally will be stabilized. If the switching is taken place far off-center, one may help to stabilize this skyrmion by just applying a stabilizer Zeeman field perpendicular to the plane of the disk. If such a field is not applied, the skyrmion will continue its motion and will collide with the disk border. The collision leads to the deformation and transformation of the skyrmion into a chiral domain wall.

The values of the stabilizer fields shown in Fig. 2 are obtained in the following way. For each point of the dynamical map we first observe where the switching is taken place and

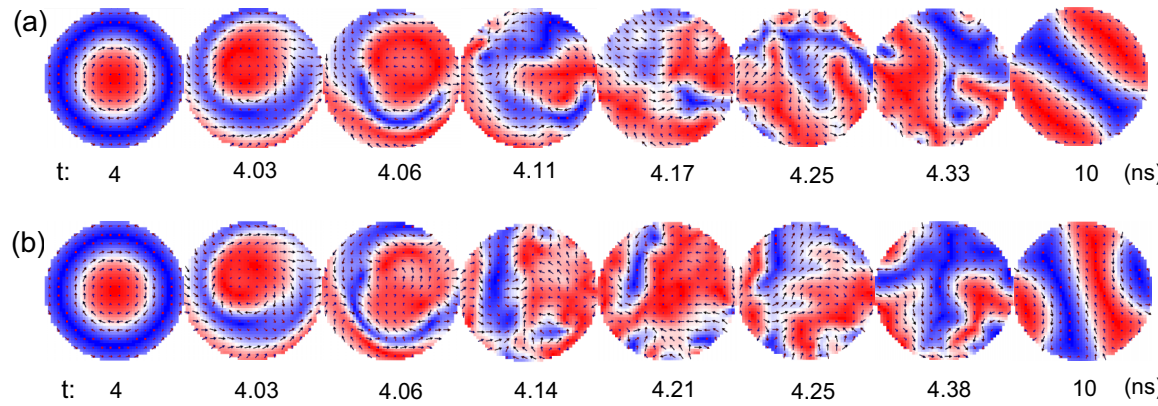

FIG. 4. The spin texture formed after application of the CMF with amplitude and frequency of (a) $H_0 = 170$ kA/m and $\nu_h = 8$ GHz and (b) $H_0 = 230$ kA/m and $\nu_h = 12$ GHz. These points are located in region IV of Fig. 2. The field is turned on at $t = 4$ ns and is turned off at $t = 4.25$ ns. After application of such CMFs the skyrmion moves rather fast, and it quickly transforms into a magnetic texture composed of three or four magnetic domains separated with domain walls of Bloch type. The sign of Q of such spin textures in most of the cases is negative (opposite to the one of the initial skyrmion).

the skyrmion is created. We then immediately switch off the CMF. In most of the cases the skyrmion is not switched near the center of the disk. The switched skyrmion has a tendency to move further towards the border of the disk. Note that the position of this skyrmion, its initial velocity, and the direction of the motion are determined by the dynamics of the system, the frequency and amplitude of the applied field. In order to prevent collisions of the switched skyrmion with the border we therefore apply a constant Zeeman field. The minimum value of such a field is plotted in Fig. 2 as the color scale. Our analysis showed that the longer the distance of this skyrmion from the disk center, the larger the amplitude of the stabilizer field. The dependence of the field on the distance is not exactly linear because it also depends on the shape of the skyrmion. In fact, in most of the cases at the moment that the skyrmion is switched, it does not possess a perfectly round shape [see for example Figs. 3(a) and 3(b)].

In Figs. 3(d) and 3(e) the trajectory of the skyrmion's guiding center before, during, and after the application of a CMF with $H_0 = 30$ kA/m and $\nu_h = 5$ GHz is presented. In order to observe the eigenmotion of the skyrmion, its initial position was defined to be at point O (1 nm, 2 nm). The skyrmion's position was then followed in time. In order to avoid effects caused by deformations and breathing, the data were recorded from point A, where the skyrmion's shape was rather circular. Owing to its up-core polarity the skyrmion starts to rotate in counterclockwise direction and finally after about 10 ns is located at the center of the disk [point B in Fig. 3(d)]. Now if one turns the CMF on, the skyrmion will follow the field direction and undergoes a clockwise motion until it disappears [the green trajectory in Fig. 3(e)]. At point C the CMF is switched off. The switched skyrmion starts to rotate in the clockwise direction with a polygon-like trajectory [shown in blue in Fig. 3(e)]. This is an indication that the core polarity of the skyrmion is down. This behavior can be well explained by the calculated skyrmion trajectory using the generalized Thiele equation, for which we derive an analytical solution in the absence and presence of CMFs and compare to the simulation results (see Sec. IV B and Fig. 5). The fact that a skyrmion with an opposite polarity exhibits an opposite trajectory may be used as the "smoking gun" of the switching.

The switching process is a result of ideal combinations of amplitude and frequency of the CMF and the confinement effects. In other words the CMF drives the skyrmion dynamics. Since the field direction is opposite to the direction of the low-frequency eigenmotion of the skyrmion, it forces the skyrmion to go through a trajectory that is opposite to its eigenmotion. The displaced skyrmion then feels the forces caused by the edge effects. The dynamical motion of the skyrmion leads to an imbalance in the system, which then results in the switching of the skyrmion. Hence the initial displacement and the frequency of the movement are decisive for the switching. If at the first moment the CMF pushes the skyrmion out of the disk area, it would result in the formation of a different magnetic order. This, in fact, covers a large part of the dynamical map and is indicated by dark blue (region IV in Fig. 2).

In order to visualize the skyrmion dynamics in region IV, we show two examples for the field amplitude and frequency of ($H_0 = 170$ kA/m, $\nu_h = 8$ GHz) and ($H_0 = 230$ kA/m, $\nu_h = 12$ GHz) in Fig. 4. As is apparent from Fig. 4 just after application of the CMF the fast movement of the skyrmion transforms it into a magnetic texture, which includes three or four magnetic domains separated with domain walls of Bloch type. Although it is rather difficult to calculate the Q number of such complex spin textures, analysis of the Q number of these magnetic textures indicates that the sign of Q in most of the cases is negative (opposite to the one of the initial skyrmion). The transformation of the skyrmion to these spin textures takes place almost immediately after the CMF is applied. This region is not therefore useful for switching, and we do not discuss it further.

As a side remark we would like to point out that calculations of the free energy of the system can eventually indicate the existence of different ground or metastale states. We have analyzed different energy terms as calculated by the micromagnetic code. Changing the frequency and amplitude of the field leads to the appearance of at least two distinct regions, i.e., switching and nonswitching regions. Each of

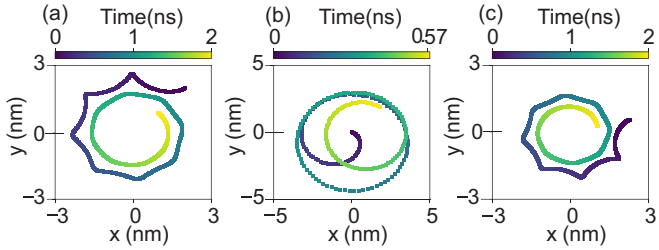

FIG. 5. The skyrmion trajectory calculated based in the generalized Thiele equation in the presence and absence of a CMF. (a) The trajectory of an up-core skyrmion when it is displaced to ($x_0 = 2$ nm, $y_0 = 2$ nm) and its motion is followed. The skyrmion starts to rotate in counterclockwise direction, and finally after a few nanosecond it stops at the center of the disk (not shown here). (b) The skyrmion trajectory in the presence of a clockwise CMF. The skyrmion rotates in the clockwise direction. The trajectory is plotted for the first 0.58 ns. The amplitude and frequency of the field are $H_0 = 30$ kA/m and $\nu_h = 5$ GHz, similar to the simulations. (c) The trajectory of the skyrmion after switching its core polarity. The skyrmion has a down-core polarity, and it starts to rotate in a clockwise direction, as seen in the simulations. This figure will be compared to Figs. 3(d) and 3(e), where the results of the simulations for the same skyrmion are presented.

these regions can be either a skyrmion state or a chiral domain state. This is exactly what one observes in the dynamical map of the system presented in Fig. 2.

In order to illustrate the importance of the amplitude and the frequency of CMFs, we investigated the initial displacement of skyrmion after the CMF is applied. The results were compared with those of calculations based on the extended Thiele equation. It turned out that the initial displacement is rather important. Application of a CMF primarily excites the modes associated with the gyroscopic motion of the skyrmion. This is the first and essential step towards switching. The initial motion can, in turn, excite different magnon modes in the system which can mediate the switching process. We do not exclude those effects in the switching process described here. Both the simulated as well as the calculated skyrmion motion for the first few tenth of ns are provided in Sec. IV B.

B. Results of analytical calculation based on the Thiele equation

1. Skyrmion trajectory in the absence and presence of a CMF

In order to connect the trajectory of skyrmion observed in the simulation to the results of the Thiele equation [given by Eq. (15)] one needs to know the mass of the skyrmion $\mathcal{M}$ and the spring constant $\mathcal{K}$. As discussed in Ref. [58], one can express $\mathcal{M}$ and $\mathcal{K}$ in terms of the eigenfrequencies of the system

$$\mathcal{M} = \frac{-\mathcal{G}}{\omega_1 + \omega_2}, \tag{16}$$

$$\tilde{\mathcal{K}} = -\omega_1\omega_2 + \left(\frac{\tilde{\mathcal{D}}}{2}\right)^2 \tag{17}$$

We use the two eigenfrequencies of skyrmion obtained from the simulation results, $2\pi\nu_1$ and $2\pi\nu_2$. The values of $\mathcal{M}$ and $\tilde{\mathcal{K}}$ will then be 1.3×10^{-24} kg and 2.6×10^{20} J/(m^{2}kg), respectively. Considering $\xi \simeq 1$, the value of μ will be about 0.15×10^{-15} kg m^2/(A/s^2). The value of $\mathcal{G}$ is about 0.47×10^{-13} Js/m^2. The value of the dissipation term $\tilde{\mathcal{D}}$ will be about 0.9×10^{10} s^{-1} using a numerical calculation of Eq. (4). However, a better agreement with the simulation results was found by considering a smaller value of $\tilde{\mathcal{D}} = 0.25 \times 10^{10}$ s^{-1}. This might be due to the boundary effects, which act as additional forces on the confined skyrmion or changes in the shape of the skyrmion during its motion.

In order to check the validity of our assumptions we first calculated the skyrmion trajectory in the absence of the CMF. Figure 5(a) presents the trajectory of an up-core skyrmion calculated using the extended Thiele equation during 2 ns in the absence of the CMF and with the initial position of $x_0 = 2$ nm and $y_0 = 2$ nm, showing the well-known polygon-like trajectory. The overall motion of the skyrmion in this case is counterclockwise, as expected.

Now we consider a clockwise CMF and calculate the skyrmion trajectory in the presence of such a field. The results for the first 0.58 ns are presented in Fig. 5(b). The amplitude and frequency of the field are $H_0 = 30$ kA/m and $\nu_h = 5$ GHz, similar to the ones used for our simulations. One observes that the skyrmion follows the field direction, as expected. For the sake of completeness we also calculate the trajectory of the skyrmion after switching its core polarity. To do so one needs to rewrite Eq. (2) for a down-core skyrmion and calculate the trajectory in the exact same way discussed above. The results of such calculations are provided in Fig. 5(c). The skyrmion with a down-core polarity rotates in clockwise direction. This is exactly what one observes in the simulations [see the results shown in Figs. 3(d) and 3(e)].

2. The initial displacement of the skyrmion in the presence of a CMF

As is discussed in Sec. III the dynamical switching of the skyrmion polarity depends on its displacement from the center of the nanodisk when the CMF is applied. This displacement depends strongly on the amplitude and the frequency of the CMF. We define the skyrmion displacement from the disk center as

$$R(t) = \sqrt{x^2(t) + y^2(t)}, \tag{18}$$

where x and y describe the skyrmion position in Cartesian coordinates and are given by Eq. (15). In order to demonstrate how this quantity depends on the amplitude and frequency of the CMF, we obtain this quantity from both micromagnetic simulations and the analytical calculations and compare the results. In order to determine the displacement of the skyrmion from the simulations, we take snapshots at different time frames after application of the CMF. Depending on the frequency of the CMF we use an appropriately small time step in order to obtain enough data. The guiding center then is defined as the place where the center of the up-domain is located. We track the position of this guiding center as a function of time.

For calculating the displacement according to the extended Thiele equation one requires the physical constants as discussed in Sec. III. After inserting those values into Eqs. (11)–(15) one obtains the x and y position of the

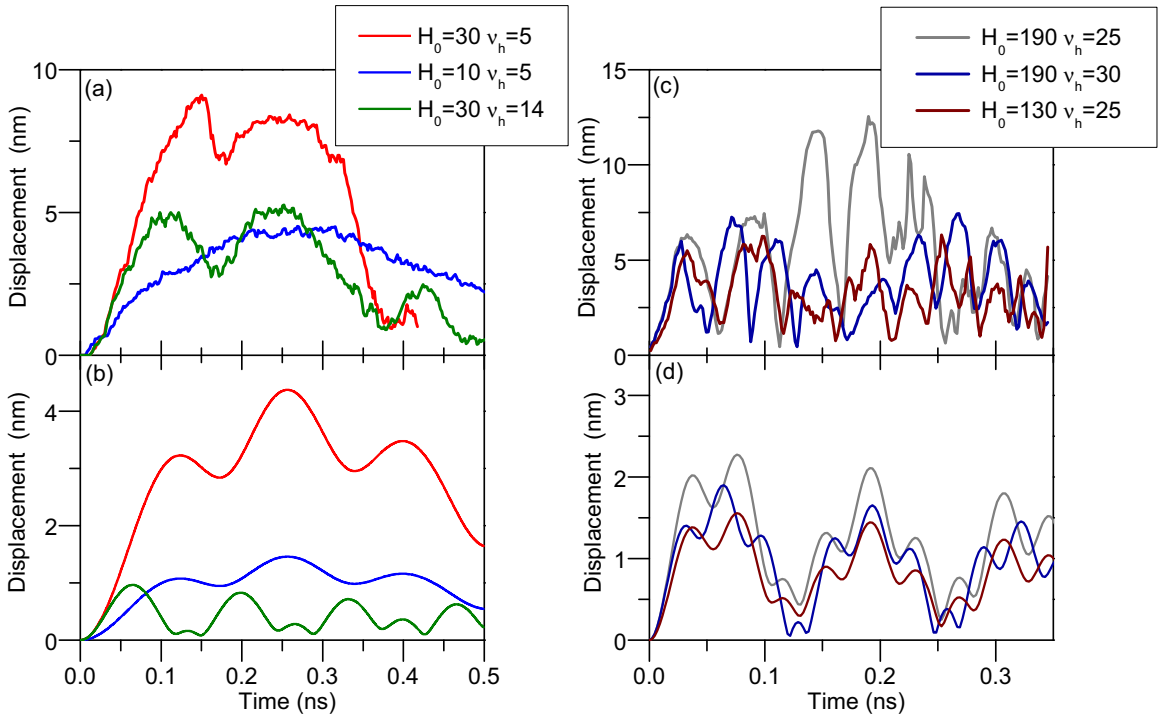

FIG. 6. The displacement of the skyrmion from the disk center during application of different CMFs. The results of low- and mid-frequency fields are shown in (a) and (b). The results of high-frequency fields are shown in (c) and (d). The results of simulation are presented in (a) and (c). The results of calculations, based on the extended Thiele equation, are shown in (b) and (d). H_0 denotes the amplitude of CMF, and $\nu_h = \omega_h/2\pi$ denotes its frequency. The values of H_0 and ν_h are given in kA/m and GHz, respectively.

skyrmion in the Cartesian coordinate. The displacement is then calculated according to Eq. (18).

The results for a few points within the dynamical map, representing different regions, are presented in Fig. 6. We first show the results for a few points near the region IIIA of Fig. 2. Near this region since the frequency of the CMF is rather low, the skyrmion motion is rather slow, but the displacement from the center of the disk is rather large. At a given frequency, the larger the field amplitude the larger the displacement. This fact can be concluded from both simulated [Fig. 6(a)] and calculated [Fig. 6(b)] displacement. At higher frequencies the motion is fast and is mainly confined near the center. This behavior is observed for both the simulated [Fig. 6(c)] as well as the calculated [Fig. 6(d)] skyrmion displacement. Since at higher frequencies the displacement is small, the skyrmion is less affected by the boundary effects. Hence, it is more stable over a larger range of the field amplitudes. Note that differences between the results of calculation and simulation shown in Fig. 6 stem from the fact that in the calculations we just estimate the values of the physical constants appearing in the extended Thiele equation. These values may differ quantitatively from the actual values involved in the micromagnetic simulations. In addition, in the analysis based on the extended Thiele equation changes in the boundary conditions and the skyrmion size as a result of the applied CMF have not been taken into consideration. The changes in the size and the shape of the skyrmion are more dramatic at higher frequencies and higher field amplitudes.

C. Dependence of the dynamical map on the disk parameters

Details of the H_0-ν_h dynamical map presented in Fig. 2 depend on the disk parameters (see discussion below). Generally a large variety of materials can host magnetic skyrmions. In order to have an idea in which materials the switching of the core polarity is favored, one needs to discuss the effects of the disk parameters on the dynamical map. As a simple illustration, we choose an effective magnetic anisotropy constant which is about 1.5 times larger than the value used above. With this anisotropy constant $K = 0.27 \times 10^6$ J/m^3, the critical value of the DM constant needed to stabilize the skyrmion in the ground state will also be larger. We choose $D = 3.3 \times 10^{-3}$ J/m^2 in the present case. Considering the same material parameters ($M_s = 1.1 \times 10^6$A/m and $A = 16 \times 10^{-12}$ J/m) one can stabilize an up-core skyrmion located at the center of the disk. We aim to observe possible changes in the switching process of this skyrmion. We first measure the eigenfrequencies of the skyrmion before application of any CMF. To do so we apply a Gaussian pulse field with an amplitude of 143 kA/m and a pulse width of 65 ps along the x direction. The skyrmion moves to the position $(x, y) \approx (2.5$ nm, 2 nm). Now we track the skyrmion trajectory during the time. In order to avoid the effects caused by the field, the data are recorded 0.62 ns after application of the field. Figure 7 shows the trajectory of skyrmion and the FFT power spectrum of its coordinates. The results indicate that this skyrmion possesses eigenfrequencies of $\nu_1 = 1$ GHz and $\nu_2 = 8.8$ GHz, slightly larger than those of the skyrmion stabilized with smaller K and D. It is interesting to figure out how this shift in the

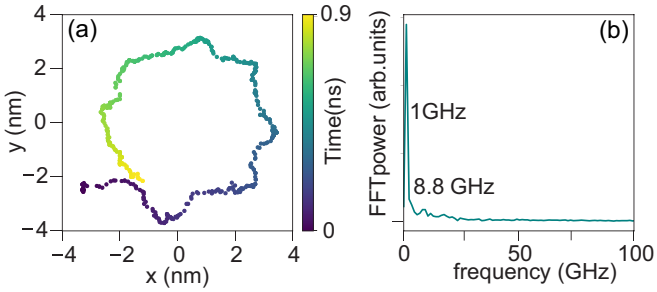

FIG. 7. (a) Trajectory of the skyrmion stabilized with $K = 0.27 \times 10^6$ J/m^3 and $D = 3.3 \times 10^{-3}$ J/m^2 driven by a Gaussian pulse field with the width of 65 ps and the magnitude of about 143 kA/m. In order to avoid the effects caused by the field, the data are recorded 0.62 ns after application of the field. The trajectory is obtained from the micromagnetic simulations and is recorded for 0.9 ns. (b) The FFT results of the x and y coordinates of the skyrmion's guiding center.

eigenfrequencies causes changes in the amplitude of the CMF required for switching.

Now we apply CMFs with different frequencies and amplitudes to the system and investigate the dynamics of the skyrmion. We are interested in the frequencies in the vicinity of the eigenfrequency of the skyrmion with the clockwise motion ($\nu_2 = 8.8$ GHz) and look for the threshold amplitude which can change the sign of the skyrmion number. We therefore applied a CMF with a frequency in the range $\nu_h = 5$–10 GHz and the amplitude in the range $H_0 = 30$–100 kA/m. In the low-amplitude and low-frequency regime there is no change in the sign of Q. The minimum amplitude leading to the change of the sign of Q is about $H_0 = 60$ kA/m and at a frequency of $\nu_h = 7$ GHz. In this case, the CMF changes the Q to about -0.85 after 0.3 ns, and a skyrmion is stabilized at the center of the disk [see Figs. 8(a) and 8(b) and the related discussions]. In comparison with the case with smaller anisotropy and DM constant, the threshold field amplitude is around two times larger. This is not unexpected due to the following reasons. First, the minimum amplitude needed to observe the switching takes place for the CMFs with the frequencies near the eigenfrequency of the skyrmion with the clockwise motion. Second, for switching the core polarity an ideal combination of field amplitude and frequency is required. The larger the values of K and D the higher the amplitude of the CMF needed to change the sign of Q and consequently switch the skyrmion.

In order to see the impact of D on the switching properties one should be able to stabilize skyrmions with the same K but various values of D. Since the critical D depends on K, one should consider cases with small K in order to still be able to stabilize skyrmions with different D. We therefore choose a smaller value for K, 0.1×10^6 J/m^3. In this case we could stabilize skyrmions over a large range of D from 2.2×10^{-3} J/m^2 to 3.3×10^{-3} J/m^2. It turned out that for the skyrmion stabilized with $D = 2.2 \times 10^{-3}$ J/m^2 the switching could be realized with $H_0 = 30$ kA/m and $\nu_h = 4$ GHz. However, for the skyrmion stabilized with $D = 3.3 \times 10^{-3}$ J/m^2 application of a CMF with an amplitude and frequency of $H_0 = 30$ kA/m and $\nu_h = 4$ GHz, respectively, could not lead to any change in the sign of Q. Instead a larger H_0 and ν_h (60 kA/m and 5 GHz) were required to see the sign change of Q. This means that the threshold values of H_0 and ν_h needed to see the change in the sign of Q are moved to higher values when D was larger.

D. Possible switching of a skyrmion to a skyrmionium

As discussed in the previous section, the details of the H_0-ν_h dynamical map presented in Fig. 2 depend on the disk parameters. During the switching the skyrmion may undergo a transient state with $Q = 0$, called a skyrmionium. Under some circumstances it is possible to switch a skyrmion to a skyrmionium. This is favored for skyrmions with a large D. For such a switching in addition to the amplitude and frequency, the time duration of the CMF is also crucial.

A careful investigation of the time evolution of Q showed that for the skyrmions stabilized with large values of D one can switch them from a $Q = \pm 1$ state to a state with $Q = 0$, i.e., a skyrmionium state. In order to illustrate this interesting observation we show the results obtained for $K = 0.27 \times 10^6$ J/m^3 and $D = 3.3 \times 10^{-3}$ J/m^2 in Fig. 8. As discussed in Sec. IV C and in Fig. 7 the eigenfrequencies of the skyrmion stabilized using these parameters are $\nu_1 = 1$ GHz and $\nu_2 = 8.8$ GHz. Now using a CMF with the $H_0 = 60$ kA/m and $\nu_h = 7$ GHz one can switch the skyrmion from $Q = +1$ to $Q = -1$. Snapshots of the switching process and the evolution of the Q during the application of the CMF are shown in Figs. 8(a) and 8(b), respectively. In Fig. 8(a) the skyrmion was first stabilized for 4 ns. The field was then turned on at $t = 4$ ns and was switched off after 0.3 ns. Such a field could switch the skyrmion polarity from up to down. Figures 8(c) and 8(d) show the results for the same amplitude of CMF, $H_0 = 60$ kA/m, but with a different frequency, $\nu_h = 6$ GHz. In this case the skyrmion with $Q = +1$ was switched to a skyrmionium state with $Q = 0$. Snapshots of this process are shown in Fig. 8(c). Here again the skyrmion was stabilized for 4 ns, and then the CMF was turned on at $t = 4$ ns and was switched off after 0.3 ns. This skyrmionium state could be stabilized shortly after the field was switched off. The time evolution of the Q during the application of the CMF for 2 ns is shown in Fig. 8(d).

Such a switching to the transient skyrmionium state can be of great technological interest if the idea is to realize a three-state quantum system ($Q = +1, 0, -1$).

In order to investigate the effect of material parameters on this switching process we investigated a skyrmion stabilized with the same value of K as the one used in Sec. IV A ($K = 0.17 \times 10^6$J/m^3). We used a larger value for D and stabilized a skyrmion in the nanodisk. The value of D in the case was 3.1×10^{-3} J/m^2. It turned out that by application of a CMF with $H_0 = 30$ kA/m and $\nu_h = 6$ GHz one can switch a skyrmion with $Q = +1$ to a skyrmionium with $Q = 0$. However, in this case a stabilizer Zeeman field is needed to stabilize this skyrmionium. In addition the time duration of the CMF is very important. One should switch of the CMF just at the point where Q is zero. At this time a stabilizer Zeeman field along the core polarity of the initial skyrmion is needed in order to keep the created skyrmionium in the middle of the disk. The amplitude of this field was found to be only 4 kA/m in this case. Our results indicate that for the

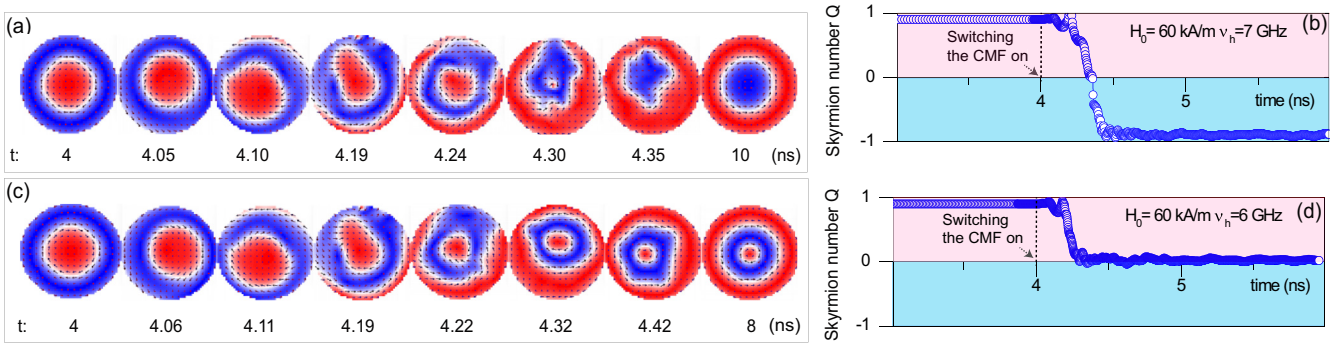

FIG. 8. Switching of a confined skyrmion with $Q = +1$ to a skyrmion with $Q = -1$ and to a skyrmionium with $Q = 0$ by a CMF. The skyrmion was stabilized with $K = 0.27 \times 10^6$ J/m^3 and $D = 3.3 \times 10^{-3}$ J/m^2. (a) Snapshots during the switching of $Q = +1$ to $Q = -1$ state. The skyrmion was first stabilized in the disk for 4 ns. It was then subjected to a clockwise CMF with $H_0 = 60$ kA/m and $\nu_h = 7$ GHz. The CMF was turned off at $t = 4.3$ ns. After turning the CMF off a down-core skyrmion with $Q = -1$ was stabilized. (b) The time evolution of the skyrmion number during the CMF with $H_0 = 60$ kA/m and $\nu_h = 7$ GHz. (c) Snapshots during the switching of $Q = +1$ to $Q = 0$ state. Again the skyrmion was initially stabilized for 4 ns. It was then subjected to a clockwise CMF with $H_0 = 60$ kA/m and $\nu_h = 6$ GHz. The CMF was turned off at $t = 4.3$ ns. After turning the CMF off a skyrmionium was created. (d) The time evolution of the skyrmion number during the CMF with $H_0 = 60$ kA/m and $\nu_h = 6$ GHz. The color scale in (a) and (c) indicates the direction of the local magnetic moments along the z direction, perpendicular to the disk (red: up, blue: down). The small arrows represent the transverse components of local moments. The CMF was applied for 2 ns in (b) and (d).

skyrmions stabilized with a larger value of D it is easier to find regions in the dynamical map, where the transient skyrmionium state can be achieved and stabilized.

V. SUMMARY

In summary we examined the stability and switching of a confined magnetic skyrmion under CMFs. A complex dynamical map was obtained including (1) regions in which the skyrmion is stable during a CMF, (2) regions in which the skyrmion collides with the border shortly after a CMF is applied, (3) switching regions in which the skyrmion core polarity is switched, and (4) regions in which the skyrmion is transformed into a different chiral magnetic order. The complex dynamics was understood by a combination of micromagnetic simulations and analysis of the extended Thiele equation. It was shown that the skyrmion is more stable at higher frequencies, since the motion is mainly confined to the central area of the disk. It was illustrated that under some circumstances a CMF can lead to the switching of the skyrmion core polarity. This switching is associated with the dynamical motion of the skyrmion. The skyrmion motion leads to the formation of domain walls at the disk border. The movement of these domain walls from the border towards the center leads to the shrinking of the initial skyrmion and creation of a skyrmion with opposite core polarity.

Our results provide guidelines for switching and manipulation of confined skyrmions using CMFs. It is important to notice that here we have demonstrated the switching of an up-core skyrmion to a down-core one. Obviously switching of a down-core skyrmion to an up-core one is also easily possible by changing the helicity of the CMF (in this case a counterclockwise field is needed). Such a switching was realized by our simulations.

Moreover, our results illustrate the stability limit of such objects under CMFs. The results are important from the perspective of data transport and storage and may be useful for realization of spintronic devices in which the dynamics and manipulation of skyrmions is the main mechanism behind the device functionality.

ACKNOWLEDGMENTS

This work was funded by the Deutscher Akademischer Austauschdienst (DAAD). The work of Kh.Z. was supported by the Deutsche Forschungsgemeinschaft (DFG) through the Heisenberg Programme ZA 902/3-1 and ZA 902/6-1 and the DFG Grant No. ZA 902/4-1. Kh.Z. thanks the Physikalisches Institut for hosting the group and providing the necessary infrastructure.

[1] J. H. Han, Skyrmions in Condensed Matter, *Springer Tracts in Modern Physics* (Springer International Publishing, Cham, 2017), Vol. 278.

[2] F. Jonietz, S. Mühlbauer, C. Pfleiderer, A. Neubauer, W. Münzer, A. Bauer, T. Adams, R. Georgii, P. Böni, R. A. Duine *et al.*, Science **330**, 1648 (2010).

[3] X. Z. Yu, N. Kanazawa, W. Z. Zhang, T. Nagai, T. Hara, K. Kimoto, Y. Matsui, Y. Onose, and Y. Tokura, Nat. Commun. **3**, 988 (2012).

[4] A. Fert, V. Cros, and J. Sampaio, Nat. Nanotech. **8**, 152 (2013).

[5] C. Song, C. Jin, J. Wang, H. Xia, J. Wang, and Q. Liu, Appl. Phys. Lett. **111**, 192413 (2017).

[6] N. Nagaosa and Y. Tokura, Nat. Nanotech. **8**, 899 (2013).

[7] G. Yu, P. Upadhyaya, Q. Shao, H. Wu, G. Yin, X. Li, C. He, W. Jiang, X. Han, P. K. Amiri *et al.*, Nano Lett. **17**, 261 (2017).

[8] A. Fert, N. Reyren, and V. Cros, Nat. Rev. Mater. **2**, 17031 (2017).

[9] O. Boulle, J. Vogel, H. Yang, S. Pizzini, D. de Souza Chaves, A. Locatelli, T. O. Menteş, A. Sala, L. D. Buda-Prejbeanu, O. Klein *et al.*, Nat. Nanotech. **11**, 449 (2016).

[10] A. Sonntag, J. Hermenau, S. Krause, and R. Wiesendanger, Phys. Rev. Lett. **113**, 077202 (2014).

[11] W. Jiang, P. Upadhyaya, W. Zhang, G. Yu, M. B. Jungfleisch, F. Y. Fradin, J. E. Pearson, Y. Tserkovnyak, K. L. Wang, O. Heinonen *et al.*, Science **349**, 283 (2015).

[12] J. Iwasaki, M. Mochizuki, and N. Nagaosa, Nat. Commun. **4**, 1463 (2013).

[13] J. Martinez, W. Lew, W. Gan, and M. Jalil, J. Magn. Magn. Mater. **465**, 685 (2018).

[14] T. Yokouchi, S. Hoshino, N. Kanazawa, A. Kikkawa, D. Morikawa, K. Shibata, T.-H. Arima, Y. Taguchi, F. Kagawa, N. Nagaosa *et al.*, Sci. Adv. **4**, eaat1115 (2018).

[15] K. Natarajan, A. Rajamani, and B. Arumugam, J. Magn. Magn. Mater. **435**, 146 (2017).

[16] A. Hrabec, J. Sampaio, M. Belmeguenai, I. Gross, R. Weil, S. M. Chérif, A. Stashkevich, V. Jacques, A. Thiaville, and S. Rohart, Nat. Commun. **8**, 15765 (2017).

[17] S. L. Zhang, W. W. Wang, D. M. Burn, H. Peng, H. Berger, A. Bauer, C. Pfleiderer, G. van der Laan, and T. Hesjedal, Nat. Commun. **9**, 2115 (2018).

[18] M. Ikka, A. Takeuchi, and M. Mochizuki, Phys. Rev. B **98**, 184428 (2018).

[19] F. Büttner, I. Lemesh, M. Schneider, B. Pfau, C. M. Günther, P. Hessing, J. Geilhufe, L. Caretta, D. Engel, B. Krüger *et al.*, Nat. Nanotech. **12**, 1040 (2017).

[20] M. Ezawa, Phys. Rev. Lett. **105**, 197202 (2010).

[21] S. Mühlbauer, B. Binz, F. Jonietz, C. Pfleiderer, A. Rosch, A. Neubauer, R. Georgii, and P. Böni, Science **323**, 915 (2009).

[22] S.-Z. Lin, A. Saxena, and C. D. Batista, Phys. Rev. B **91**, 224407 (2015).

[23] A. O. Leonov and I. Kézsmárki, Phys. Rev. B **96**, 014423 (2017).

[24] M. Vousden, M. Albert, M. Beg, M.-A. Bisotti, R. Carey, D. Chernyshenko, D. Cortés-Ortuño, W. Wang, O. Hovorka, C. H. Marrows *et al.*, Appl. Phys. Lett. **108**, 132406 (2016).

[25] T. Okubo, S. Chung, and H. Kawamura, Phys. Rev. Lett. **108**, 017206 (2012).

[26] Y. Hu, X. Chi, X. Li, Y. Liu, and A. Du, Sci. Rep. **7**, 16079 (2017).

[27] S. Heinze, K. von Bergmann, M. Menzel, J. Brede, A. Kubetzka, R. Wiesendanger, G. Bihlmayer, and S. Blügel, Nat. Phys. **7**, 713 (2011).

[28] C. Jin, Z.-A. Li, A. Kovács, J. Caron, F. Zheng, F. N. Rybakov, N. S. Kiselev, H. Du, S. Blügel, M. Tian *et al.*, Nat. Commun. **8**, 15569 (2017).

[29] S. Gupta and A. Saxena, *The Role of Topology in Materials*, Springer Series in Solid-State Sciences (Springer International Publishing, Cham, 2018), Vol. 189.

[30] S. Rohart and A. Thiaville, Phys. Rev. B **88**, 184422 (2013).

[31] R. Juge, S.-G. Je, D. de Souza Chaves, S. Pizzini, L. D. Buda-Prejbeanu, L. Aballe, M. Foerster, A. Locatelli, T. O. Menteş, A. Sala *et al.*, J. Magn. Magn. Mater. **455**, 3 (2018).

[32] N. Ran, G. P. Zhao, H. Tang, L. C. Shen, P. Lai, J. Xia, X. Zhang, and Y. Zhou, AIP Adv. **7**, 025105 (2017).

[33] D. Cortés-Ortuño, N. Romming, M. Beg, K. von Bergmann, A. Kubetzka, O. Hovorka, H. Fangohr, and R. Wiesendanger, Phys. Rev. B **99**, 214408 (2019).

[34] R. Novak, F. Garcia, E. Novais, J. Sinnecker, and A. Guimarães, J. Magn. Magn. Mater. **451**, 749 (2018).

[35] R. Keesman, A. O. Leonov, P. van Dieten, S. Buhrandt, G. T. Barkema, L. Fritz, and R. A. Duine, Phys. Rev. B **92**, 134405 (2015).

[36] J. Mulkers, K. M. D. Hals, J. Leliaert, M. V. Milošević, B. Van Waeyenberge, and K. Everschor-Sitte, Phys. Rev. B **98**, 064429 (2018).

[37] F. Büttner, I. Lemesh, and G. S. D. Beach, Sci. Rep. **8**, 4464 (2018).

[38] H. Du, R. Che, L. Kong, X. Zhao, C. Jin, C. Wang, J. Yang, W. Ning, R. Li, C. Jin *et al.*, Nat. Commun. **6**, 8504 (2015).

[39] G. Finocchio, F. Büttner, R. Tomasello, M. Carpentieri, and M. Kläui, J. Phys. D **49**, 423001 (2016).

[40] Z. V. Gareeva and K. Y. Guslienko, Phys. Solid State **60**, 1146 (2018).

[41] A. Talapatra and J. Mohanty, Comput. Mater. Sci. **154**, 481 (2018).

[42] Y. F. Chen, Z. X. Li, Z. W. Zhou, Q. L. Xia, Y. Z. Nie, and G. H. Guo, J. Magn. Magn. Mater. **458**, 123 (2018).

[43] K. Y. Guslienko and Z. V. Gareeva, IEEE Magn. Lett. **8**, 1 (2017).

[44] I. Makhfudz, B. Krüger, and O. Tchernyshyov, Phys. Rev. Lett. **109**, 217201 (2012).

[45] F. Zheng, H. Li, S. Wang, D. Song, C. Jin, W. Wei, A. Kovács, J. Zang, M. Tian, Y. Zhang *et al.*, Phys. Rev. Lett. **119**, 197205 (2017).

[46] Y. Liu, H. Du, M. Jia, and A. Du, Phys. Rev. B **91**, 094425 (2015).

[47] C. Heo, N. S. Kiselev, A. K. Nandy, S. Blügel, and T. Rasing, Sci. Rep. **6**, 27146 (2016).

[48] M. Schott, A. Bernand-Mantel, L. Ranno, S. Pizzini, J. Vogel, H. Béa, C. Baraduc, S. Auffret, G. Gaudin, and D. Givord, Nano Lett. **17**, 3006 (2017).

[49] B. Zhang, W. Wang, M. Beg, H. Fangohr, and W. Kuch, Appl. Phys. Lett. **106**, 102401 (2015).

[50] M. Curcic, B. Van Waeyenberge, A. Vansteenkiste, M. Weigand, V. Sackmann, H. Stoll, M. Fähnle, T. Tyliszczak, G. Woltersdorf, C. H. Back *et al.*, Phys. Rev. Lett. **101**, 197204 (2008).

[51] A. A. Thiele, Phys. Rev. Lett. **30**, 230 (1973).

[52] M. J. Donahue and D. G. Porter (1999), OOMMF User's Guide Version 1.0. (National Institute of Standards and Technology, Gaithersburg, MD, 1999), http://math.nist.gov/oommf/.

[53] A. Bogdanov and A. Hubert, J. Magn. Magn. Mater. **138**, 255 (1994).

[54] A. Thiaville, S. Rohart, M. Jué, V. Cros, and A. Fert, Europhys. Lett. **100**, 57002 (2012).

[55] J. Sampaio, V. Cros, S. Rohart, A. Thiaville, and A. Fert, Nat. Nanotech. **8**, 839 (2013).

[56] L. Camosi, N. Rougemaille, O. Fruchart, J. Vogel, and S. Rohart, Phys. Rev. B **97**, 134404 (2018).
[57] A. Thiaville, J. M. García, R. Dittrich, J. Miltat, and T. Schrefl, Phys. Rev. B **67**, 094410 (2003).
[58] K.-W. Moon, B. S. Chun, W. Kim, Z. Q. Qiu, and C. Hwang, Phys. Rev. B **89**, 064413 (2014).
[59] K. Y. Guslienko, B. A. Ivanov, V. Novosad, Y. Otani, H. Shima, and K. Fukamichi, J. Appl. Phys. **91**, 8037 (2002).
[60] K. Y. Guslienko, V. Novosad, Y. Otani, H. Shima, and K. Fukamichi, Appl. Phys. Lett. **78**, 3848 (2001).
[61] J. Burgess, J. Losby, and M. Freeman, J. Magn. Magn. Mater. **361**, 140 (2014).